

Article

# Analysis of Resistance Characteristics and Research into Resistance Reduction of a Tee Based on Field Synergy

Yajing Yan, Chongfang Song \*, Wuxuan Pan, Jie Wang and Yifan Bai

School of Civil Engineering, Taiyuan University of Technology, Taiyuan 030024, China;  
yanyajing0552@link.tyut.edu.cn (Y.Y.); wuxuanpan@tyut.edu.cn (W.P.); wangjie0556@link.tyut.edu.cn (J.W.);  
baiyifan0871@link.tyut.edu.cn (Y.B.)

\* Correspondence: songchongfang@tyut.edu.cn

**Abstract:** The resistance loss and energy consumption when fluid flows through a tee in an HVAC system are severe. To improve energy efficiency and reduce carbon emissions, a novel tee with a U-shaped deflector is proposed, supported by experiments and numerical simulations. The resistance reduction mechanism of the U-shaped deflector was analyzed according to the viscous dissipation principle and the field synergy principle. The resistance reduction of the novel tee with different deflector angles and a traditional tee were compared. The results show that the resistance loss of the tee was mainly due to the flow separation and deformation of the fluid in the main branch. The relationship between the local resistance coefficient and the diameter ratio of the main-branch pipe was exponential, and the relationship between the local resistance coefficient and the diameter ratio of the main straight pipe was linear. The total resistance loss reduction rate of the tee with the addition of a 26° deflector was the highest, reaching 72.4%, the volume-weighted average synergy angle increased by 1°, and the viscous dissipation decreased by 21.7%. This study provides a reference for the resistance reduction design of complex local components such as tees in HVAC systems.

**Keywords:** resistance loss; T-tee; field synergy; viscous dissipation; deflector; resistance reduction



**Citation:** Yan, Y.; Song, C.; Pan, W.; Wang, J.; Bai, Y. Analysis of Resistance Characteristics and Research into Resistance Reduction of a Tee Based on Field Synergy. *Buildings* **2024**, *14*, 1271. <https://doi.org/10.3390/buildings14051271>

Academic Editor: Antonio Caggiano

Received: 16 March 2024

Revised: 21 April 2024

Accepted: 28 April 2024

Published: 1 May 2024



**Copyright:** © 2024 by the authors. Licensee MDPI, Basel, Switzerland. This article is an open access article distributed under the terms and conditions of the Creative Commons Attribution (CC BY) license (<https://creativecommons.org/licenses/by/4.0/>).

## 1. Introduction

With the acceleration of global warming, people are increasingly concerned about carbon emissions. However, there is a relationship between energy consumption and carbon emissions. Reducing energy consumption and improving energy efficiency are beneficial for reducing carbon emissions [1,2]. Energy consumption in buildings accounts for 30% of global energy consumption. Operational energy consumption is an important component of energy consumption in buildings [3,4]. With the improvement of people's living standards and indoor environment requirements, operational energy consumption in buildings' heating, air-conditioning, ventilation (HVAC), and other systems has increased [5–7]. According to statistics, heating, air-conditioning, and ventilation (HVAC) systems account for 40–60% of a building's total energy consumption [8,9]. Local components are a necessary part of the conveying system; the resistance loss of local components is the main part of the conveying energy consumption [10]. The tee is a common local component in pipeline transportation; the flow of water flows through the irregular boundary surface of the component, and the flow pattern changes sharply, resulting in vortex. The collision, friction, and rupture of the fluid vortex consume mechanical energy [11,12]. Therefore, it is of great significance to analyze the resistance characteristics and study the resistance reduction of the tee to improve the energy efficiency and promote the energy-saving operation of buildings.

Scholars both domestically and internationally have conducted extensive research on the local resistance coefficient of tees, flow field characteristics, and methods for optimizing resistance reduction through experiments and numerical simulations [13–15]. Gardel et al. [16] experimentally investigated the local resistance coefficients of merge tees,

taking into account the effects of branch angle and curvature, and derived a semi-empirical expression for a merge tee. Miller [17] experimentally studied split-flow and merge tee pipelines with different shapes, starting with the geometry and flow rate of the tee. The variations in local resistance coefficient under different area ratios and flow velocity ratios were obtained. Liu et al. [18] investigated the influence of chamfer ratios and split ratios on the local resistance coefficient of tees, and analyzed the influence of chamfer radius on the local resistance of split-flow and merge tees. Han et al. [19] investigated the effects of blind tee length, end structure, and flow velocity on the flow characteristics of blind tees in laminar flow, through numerical simulations. The above research mainly focuses on the effects of flow rates, split ratios, and angle on the local resistance coefficient and flow characteristics of tees. However, the relationship between the local resistance coefficient and the pipe diameter ratio is still unclear and requires further study.

Zhang et al. [20] used numerical simulation to explore the drag reduction method of inserting deflectors in parallel pipelines and explored the drag reduction mechanism based on viscous dissipation. Gao et al. [21] studied the influence of changing the wall radian of the tee on the resistance loss of the tee from the perspective of viscous dissipation and verified the drag reduction effect through experiments. Yin et al. [22] used experiments and numerical simulations based on viscous dissipation and eddy current strength and analyzed the resistance loss of the tee after changing the radius of the inner and outer corners of the branch pipe. Jing et al. [23] optimized the wall curvature of a tee based on the gradient descent method, proposed a transitional tee, and studied the resistance reduction rate of the transitional tee under different flow and area ratios. Most of the previous studies have discussed only one optimization method. Thus, the resistance reduction effect of a combination of multiple optimization methods remains to be studied.

Guo et al. [24] studied the interaction between the velocity field and the temperature gradient field in the flow field. They pointed out that heat transfer can be enhanced by reducing the angle between the velocity field and the temperature gradient field and proposed the field synergy principle. At present, the field synergy principle is not only widely used to enhance heat transfer, but also has been rapidly developed and applied in the field of flow [25–29]. Chen et al. [30] found that flow resistance was related to the synergy degree of velocity and velocity gradient, and established the field synergy equation for fluid flow, which provides theoretical guidance for the study of flow resistance reduction. Subsequently, other researchers conducted further research on the basis of this research method. Yin et al. [31] proposed the synergistic principle of compressible flow field and found that reducing the synergistic performance of the velocity vector and density logarithmic gradient in microchannels could reduce fluid resistance. Yin et al. [32] analyzed the resistance reduction mechanism of the deflector elbow based on the field synergy principle and verified that the synergy of the velocity and pressure gradient could be used to evaluate the resistance characteristics of local components. At present, research on resistance reduction through field synergy is mainly aimed at elbows, micro-channels, and other components. However, research on complex local components such as tees is relatively lacking.

This study analyzed the resistance characteristics of a tee through experiments and numerical simulations, obtaining the relationship between the local resistance coefficient and pipe diameter ratio, and a novel tee with a U-shaped deflector is proposed. The resistance reduction mechanisms of different forms of U-shaped deflectors were analyzed through viscous dissipation and field synergy, and the resistance reduction effects of a novel tee with different deflector angles were compared. This study provides a technical path for the study of resistance reduction in complex components such as tees in HVAC systems.

## 2. Numerical Simulation and Experiment

### 2.1. Numerical Simulation

#### 2.1.1. Establishment of the Geometric Model

The geometric model of the horizontal T-tee is shown in Figure 1. The main pipe diameter  $D$  is 40 mm, and the straight pipe diameter  $D$  is 40 mm. In order to obtain the flow resistance under different pipe diameter ratios, five working conditions with branch pipe diameters  $d$  of 15 mm, 20 mm, 25 mm, 32 mm, and 40 mm were studied. The calculation area selected upstream  $20D$ , downstream  $20D$ , and branch  $20d$  tube lengths that had almost no effect on the flow in the tee. The calculated cross-sections of pressure and velocity are shown in 0-0, 1-1, and 2-2 in Figure 1.

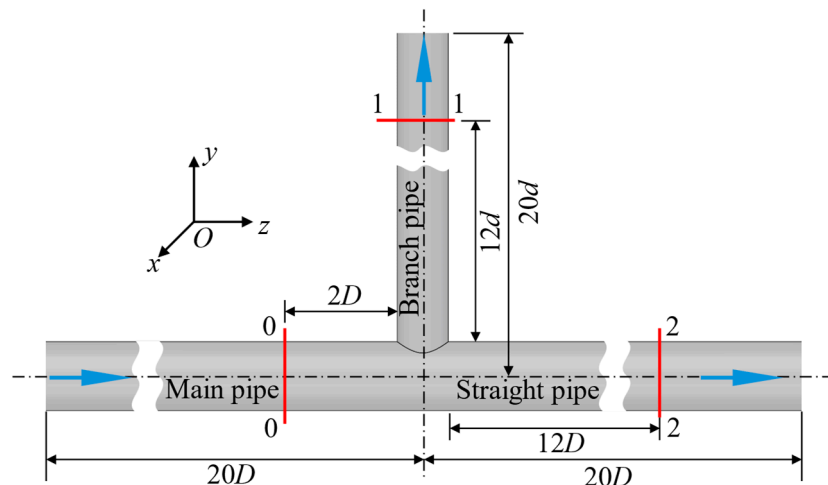


**Figure 1.** Tee geometric model diagram.

#### 2.1.2. Turbulent Flow Model

The realizable  $k-\varepsilon$  model can effectively consider the effect of secondary flow caused by fluid deformation and well reflects the flow characteristics of fluid separation and reflux [33]. Therefore, the realizable  $k-\varepsilon$  turbulence model was selected in this study.

The flow control equation is as follows:

The continuous equation is as follows:

$$\frac{\partial u_j}{\partial x_j} = 0 \quad (1)$$

The momentum equation is as follows:

$$\rho u_j \frac{\partial u_i}{\partial x_j} = -\frac{\partial p}{\partial x_i} + \frac{\partial}{\partial x_j} \left( \mu \frac{\partial u_i}{\partial x_j} - \rho u'_i u'_j \right) \quad (2)$$

The turbulent kinetic energy ( $k$ ) is as follows:

$$\rho u_j \frac{\partial k}{\partial x_j} = \frac{\partial}{\partial x_j} \left[ \left( \mu + \frac{\mu_t}{\sigma_k} \right) \frac{\partial k}{\partial x_j} \right] + G_k + G_b - \rho \varepsilon - Y_M + S_k \quad (3)$$

The turbulence dissipation rate ( $\varepsilon$ ) is as follows:

$$\rho u_j \frac{\partial \varepsilon}{\partial x_j} = \frac{\partial}{\partial x_j} \left[ \left( \mu + \frac{\mu_t}{\sigma_\varepsilon} \right) \frac{\partial \varepsilon}{\partial x_j} \right] + C_{1\varepsilon} \frac{\varepsilon}{k} (G_k + C_{3\varepsilon} G_b) - C_{2\varepsilon} \rho \frac{\varepsilon^2}{k} + S_\varepsilon \quad (4)$$

The turbulent viscosity ( $\mu_t$ ) is as follows:

$$\mu_t = \rho C_\mu \frac{k^2}{\varepsilon} \quad (5)$$

where  $u_i$  and  $u_j$  are the velocities in the x and y directions,  $k$  is the turbulent kinetic energy,  $\varepsilon$  is the turbulent dissipation rate,  $C_{1\varepsilon}$  and  $C_{2\varepsilon}$  are empirical constants, which are 1.44 and 1.92, respectively, and  $\sigma_k$  and  $\sigma_\varepsilon$  are the Prandtl numbers corresponding to the turbulent kinetic energy and turbulent dissipation rate, which are 1.0 and 1.3, respectively [20].

### 2.1.3. Meshing and Boundary Conditions

The irregular shape of the tee made the internal flow pattern uneven. The complex flow was difficult to calculate in a single sub-region, so the computational region was divided into four regions as shown in Figure 2. The inlet of the main pipe was the velocity inlet, the inlet velocity was 0.5 m/s, and the straight pipe and the branch pipe were set to free outflow. The SIMPLE algorithm was used to solve the pressure and velocity coupling. The discrete formats of momentum, turbulent kinetic energy, and dissipation rate adopted the second-order upwind format, and the wall function method was used to calculate the flow in the side wall area. The normalized residual value of each parameter was  $10^{-5}$ .

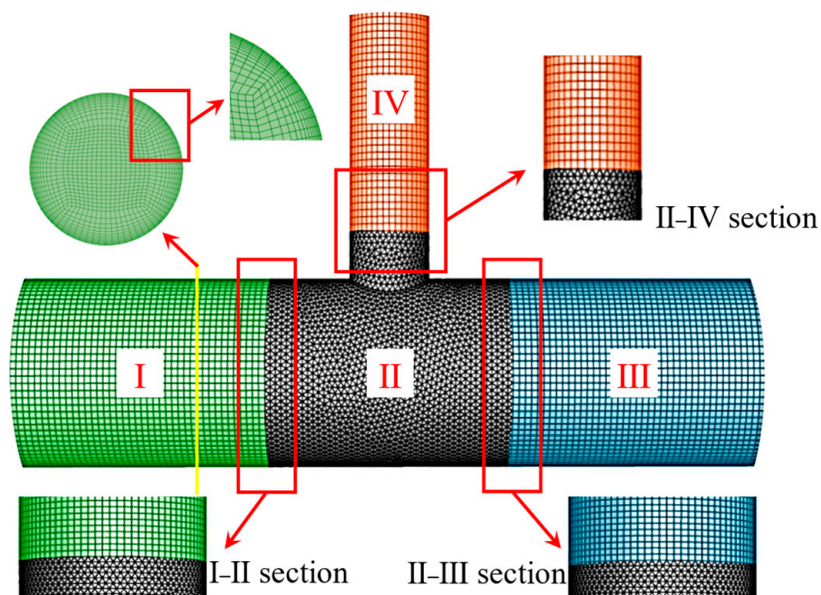


**Figure 2.** Grid generation.

### 2.2. Experimental Research

The experimental tee device is shown in Figure 3. The diameter of the experimental tube was 40 mm. The pump was started. After the constant pressure water tank (5) overflowed, the flow regulation valve (7) was closed, the residual gas in the experimental tee pipe was exhausted, and we waited for the liquid level of the pressure measuring pipe ①~⑨ to be flush. The flow rate was adjusted by opening the regulation valve (7) and measured using the weighing method. Once the liquid level in the pressure measuring tube had stabilized, the head heights of pressure measuring tubes ①~⑨ were measured and recorded using a pressure gauge (12).

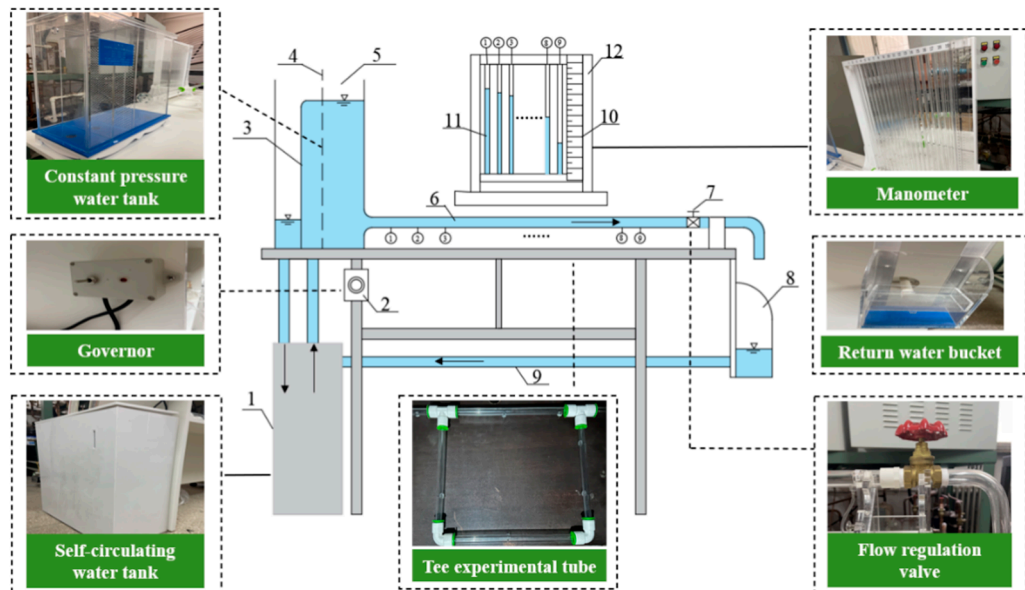


**Figure 3.** Diagram of the local resistance loss experimental tee device.

### 2.3. Field Synergy Principle

Based on the synergy theory of the velocity field and temperature field, He [34] analyzed the synergistic relationship between the velocity field and pressure gradient field and found that the synergy of the velocity field and pressure gradient field is beneficial for evaluating the resistance loss.

For incompressible fluids without external force, the momentum equation of the fluid flow process is as follows:

$$\rho \vec{U} \cdot \nabla \vec{U} = -\nabla P + \mu \nabla^2 \vec{U} \quad (6)$$

Multiplying both sides of Equation (6) by the velocity vector  $\vec{U}$ :

$$-\vec{U} \cdot \nabla P = \left( \rho \vec{U} \cdot \nabla \vec{U} - \mu \nabla^2 \vec{U} \right) \cdot \vec{U} \quad (7)$$

the dot product equation of Equation (7) is as follows:

$$-|U||\nabla P| \cos \theta = |\rho U \cdot \nabla U - \mu \nabla^2 U| |U| \cos \theta \quad (8)$$

Integrating the entire flow field yields the following:

$$\iiint_{\Omega} -|U||\nabla P| \cos \theta dV = \iiint_{\Omega} |\mu \nabla^2 U - \rho U \cdot \nabla U| |U| \cos \theta dV \quad (9)$$

According to (7) and (8), the synergistic relationship between the velocity field and the pressure gradient field is as follows:

$$-\vec{U} \cdot (\nabla P) = -|U||\nabla P| \cos \theta \quad (10)$$

$$\theta' = \arccos \left[ \frac{u_x \left( \frac{\partial p}{\partial x} \right) + u_y \left( \frac{\partial p}{\partial y} \right) + u_z \left( \frac{\partial p}{\partial z} \right)}{\sqrt{u_x^2 + u_y^2 + u_z^2} \sqrt{\left( \frac{\partial p}{\partial x} \right)^2 + \left( \frac{\partial p}{\partial y} \right)^2 + \left( \frac{\partial p}{\partial z} \right)^2}} \right] \quad (11)$$

The volume-weighted average synergy angle  $\bar{\theta}$  is as follows:

$$\bar{\theta} = \frac{\iiint_{\Omega} \theta' dV}{\iiint_{\Omega} dV} \quad (12)$$

The cross-section average synergy angle  $\bar{\theta}'$  is as follows:

$$\bar{\theta}' = \frac{\iint_{\Gamma} \theta' dS}{\iint_{\Gamma} dS} \quad (13)$$

#### 2.4. Determination of the Local Resistance Coefficient

As shown in Figure 1, the pressures of sections 0-0, 1-1, and 2-2 were  $P_0$ ,  $P_1$ , and  $P_2$ , respectively; the pressure difference between the 0-0 and 1-1 sections of the main-branch pipe was  $\Delta P_{01}$ , and the local resistance coefficient was  $\zeta_{01}$ . The pressure difference between the 0-0 and 2-2 sections of the main straight pipe was  $\Delta P_{02}$ , and the local resistance coefficient was  $\zeta_{02}$ .  $u_0$ ,  $u_1$ , and  $u_2$  were the velocities of the main pipe, branch pipe, and straight pipe, respectively.

According to the energy equation, the calculation formulas of the local resistance coefficient of the tee are [22] as follows:

$$P_0 + \frac{1}{2}\rho u_0^2 = P_1 + \frac{1}{2}\rho u_1^2 + \lambda_0 \frac{l_0}{D} \rho \frac{u_0^2}{2} + \lambda_1 \frac{l_1}{d} \rho \frac{u_1^2}{2} + \Delta P_{01} \quad (14)$$

$$P_0 + \frac{1}{2}\rho u_0^2 = P_2 + \frac{1}{2}\rho u_2^2 + \lambda_0 \frac{l_0}{D} \rho \frac{u_0^2}{2} + \lambda_2 \frac{l_2}{D} \rho \frac{u_2^2}{2} + \Delta P_{02} \quad (15)$$

where  $\rho$  is  $997 \text{ kg/m}^3$ . The resistance coefficient  $\lambda$  of different pipe sections was determined as follows:  $\lambda = 0.3164/\text{Re}^{0.25}$  ( $4 \times 10^3 < \text{Re} < 1 \times 10^5$ ),  $\lambda = 0.0032 + 0.221\text{Re}^{-0.237}$  ( $1 \times 10^5 < \text{Re} < 3 \times 10^6$ ).

Therefore, the local resistance coefficients of the two flow directions are as follows:

$$\zeta_{01} = \frac{\Delta P_{01}}{\frac{1}{2}\rho u_0^2} \quad (16)$$

$$\zeta_{02} = \frac{\Delta P_{02}}{\frac{1}{2}\rho u_0^2} \quad (17)$$

#### 2.5. Grid Independence Assessment and Numerical Simulation Verification

The grid division of the calculation area was carried out from sparse to dense, and the flow field in the tee under each grid section was calculated. The grid independence assessment was carried out based on the local resistance coefficient  $\zeta_{01}$ . The calculation results are shown in Figure 4. When the number of grids was greater than 1.54 million,  $\zeta_{01}$  changed little, and the change rate was only 0.6%. Therefore, it is considered that the grid met the requirements of grid independence, and the number of effective computational grids was 1.54 million.

For comparison of the numerical simulation and experimental research, taking the experiment detailed in Figure 3 as the calculation conditions, the above numerical simulation settings were used for calculation, and the flow structure in the tee was obtained. Nine measuring points were selected from the flow field results, as shown in Figure 5. The main pipe section included measuring points 1, 2, and 9; the branch pipe section included measuring points 3, 4, 5, and 6; and the straight pipe section included measuring points 7 and 8. The average head height of the pressure measuring tube at each measuring point was measured five times. Comparing the numerical simulation results of the main branch pipe and the main straight pipe with the experimental test values, the errors were found to be less than 2%. The feasibility and accuracy of the numerical simulation were confirmed by comparing the pressure values.

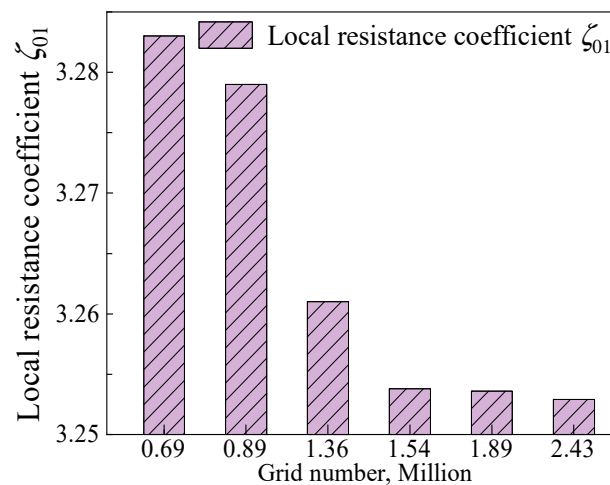


**Figure 4.** Grid independence verification.

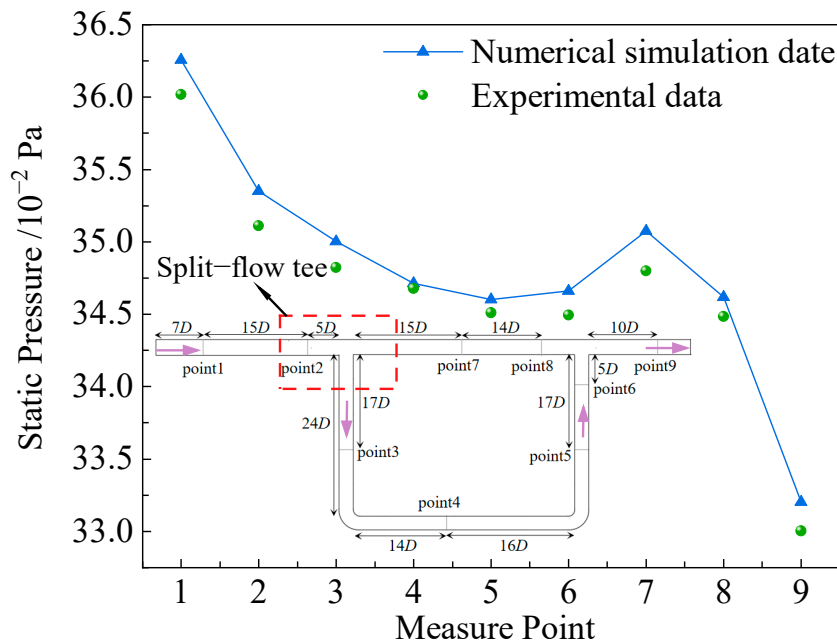


**Figure 5.** Numerical simulation and experimental comparison diagram.

Figure 5 shows that the static pressure drop at the main branch measuring points 2–3 in the tee branch was significantly greater than that at the main straight pipe measuring points 2–7. This indicates that the resistance loss at the branch was primarily concentrated in the main branch section, while the resistance loss of the main straight pipe was very small, which was also reflected in the later local resistance coefficient.

### 3. Results and Discussion

#### 3.1. Resistance Characteristics of the Split-Flow Tee

##### 3.1.1. Local Resistance Coefficient of Split-Flow Tee

Numerical simulation of the water flow in the tee was carried out. The local resistance coefficient  $\zeta$  varied with the diameter ratio  $d/D$  and the split ratio  $q$  (the ratio of flow into the branch pipe to the main pipe flow), as shown in Figure 6.

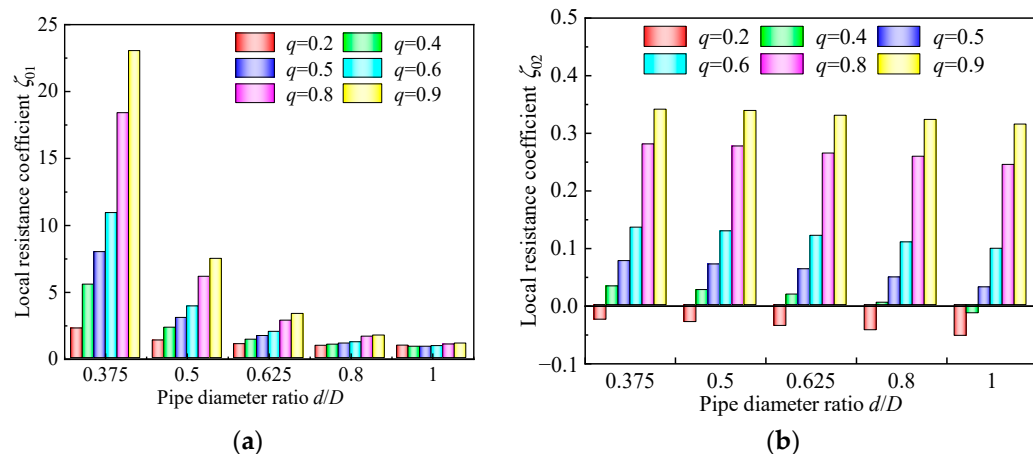


**Figure 6.** The variation of the local resistance coefficient with diameter ratio  $d/D$ : (a) the main branch pipe; (b) the main straight pipe.

Under the research conditions, the local resistance coefficient  $\zeta_{01}$  ranged from 1.4 to 23.1, while the maximum  $\zeta_{02}$  was only 0.34. This indicates that the resistance loss of the tee was primarily caused by flow separation and deformation of the fluid in the main branch.

For a specific split ratio, the local resistance coefficients  $\zeta_{01}$  and  $\zeta_{02}$  decrease as the diameter ratio  $d/D$  increases. When the split ratio is small,  $\zeta_{02}$  becomes negative due to the average kinetic energy increase caused by the fluid entering the straight pipe section being sufficient to overcome the friction between the fluid and the wall as well as the wall shear force.

When using the design manual for pipeline hydraulic calculations, it is common to use a recommended value for the local resistance coefficient of the tee. However, this study found that the local resistance coefficient was related not only to the split ratio, but also to the pipe diameter ratio. Therefore, the flow field of a tee under various pipe diameter ratios was simulated and the regression equation for the local resistance coefficient of the tee and the pipe diameter ratio was derived, as shown in Table 1. The local resistance coefficient  $\zeta_{02}$  of the main straight pipe had a linear relationship with the diameter ratio  $d/D$ . The larger the split ratio  $q$ , the larger was the slope. However, the local resistance coefficient  $\zeta_{01}$  of the main branch pipe did not show a simple linear relationship with the diameter ratio  $d/D$ , and this was found to be a power exponential relationship. The larger the split ratio  $q$ , the greater was the absolute value of the negative index, and the more severe the influence on  $\zeta_{01}$ . This law is also consistent with the results shown in Figure 6a.

**Table 1.** Regression equation for the diameter ratio  $d/D$  and local resistance coefficient  $\zeta$ .

$q$	The Regression Equation of $d/D$ and $\zeta$	$R^2$
0.2	$\zeta_{01} = 0.7149 \times (d/D)^{-1.08967}$	0.8919
	$\zeta_{02} = -0.0462 \times (d/D)^{-0.0072}$	0.9973
0.4	$\zeta_{01} = 0.4479 \times (d/D)^{-2.54005}$	0.9781
	$\zeta_{02} = -0.0755 \times (d/D) + 0.0634$	0.9826
0.5	$\zeta_{01} = 0.4196 \times (d/D)^{-2.98756}$	0.9888
	$\zeta_{02} = -0.0741 \times (d/D) + 0.1068$	0.9860
0.6	$\zeta_{01} = 0.4298 \times (d/D)^{-3.28741}$	0.9937
	$\zeta_{02} = -0.0597 \times (d/D) + 0.1579$	0.9979
0.8	$\zeta_{01} = 0.5179 \times (d/D)^{-3.63463}$	0.9972
	$\zeta_{02} = -0.0580 \times (d/D) + 0.3034$	0.9748
0.9	$\zeta_{01} = 0.5649 \times (d/D)^{-3.77819}$	0.9984
	$\zeta_{02} = -0.0435 \times (d/D) + 0.3585$	0.9798

### 3.1.2. Velocity Distribution of the Split-Flow Tee

The local resistance coefficient values, above, show that the resistance loss at the branch of the tee was mainly reflected in the main branch pipe section. In order to explore the flow mechanism of energy dissipation, the fluid flow field in the tee with a split ratio of  $q = 0.5$  was numerically simulated, and the corresponding velocity field variation law was obtained. The cross-section and its velocity vector distribution are shown in Figure 7.

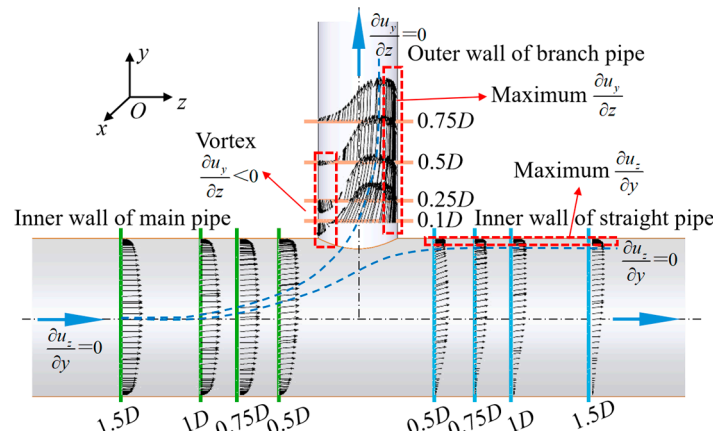


**Figure 7.** Position distribution and velocity vector diagram of each section of the tee.

The fluid at  $1.5D$  from the main pipe to the branch pipe still maintained the axisymmetric flow at the inlet, and the velocity gradient at the center line of the pipe was 0. The flow pattern changed from the  $1D$  distance between the main pipe and the branch pipe, and the flow in the main pipe began to transfer to the branch pipe. The insertion of the tee branch pipe disturbed the original axisymmetric internal flow, and the shear layer near the branch pipe side became thinner. The position of the velocity gradient of 0 shifted from the center of the main pipe to the outer wall of the branch pipe and the inner wall of the straight pipe section. Although the velocity distribution of the flow in the straight pipe section was offset with the passage of the flow, the degree of offset and the velocity gradient were small. The most significant change occurred at the branch pipe. Due to the combined action of inertial and viscous forces, the branch pipe flow was extremely uneven, and a large velocity gradient was generated in the boundary layer near the outer wall. This gradient gradually decreased from the outside to the inside, and even caused reverse vortex flow near the inner wall surface. It can be seen that in order to reduce the local resistance, it was necessary to optimize a larger velocity gradient.

### 3.2. Resistance Reduction Optimization of Split-Flow Tee

The research described above showed that the pressure loss of the tee came from the change in the internal flow field. Therefore, this study aimed to optimize the tee structure based on the synergistic relationship between the velocity field and the pressure gradient field, and then the resistance reduction effect was analyzed. Previous studies [22] have shown that the local resistance can be effectively reduced when the fillet radius of the tee is the same as the pipe diameter. In this study, the fillet radii  $R_1$  and  $R_2$  of the tee were both 20 mm. Additionally, deflectors of varying lengths were added to the outer wall of the branch pipe. Taking the  $L = 40$  mm deflector as an example, the effect of the deflector angle  $\theta$  on the local resistance of the tee ( $DN40 \times 40 \times 20$ ) was explored, as shown in Figure 8.

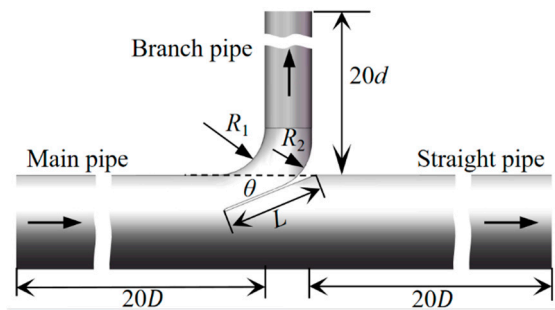


**Figure 8.** Optimized tee model.

### 3.2.1. Total Resistance Loss Coefficient of Split-Flow Tee

In order to comprehensively evaluate the local resistance coefficients of the two flows, Costa [35] proposed defining the total local resistance loss coefficient  $K$  based on the flow weight  $Q$ , which can be expressed as follows:

$$K = \zeta_{01} (Q_1/Q_0) + \zeta_{02} (Q_2/Q_0) \quad (18)$$

The reduction degree of the local resistance loss of the tee was evaluated via the reduction rate of the total local resistance loss  $\eta$ :

$$\eta = (K_0 - K)/K_0 \quad (19)$$

$K$  and  $\eta$  were calculated for the tees at six different deflector angles ( $18^\circ, 20^\circ, 22^\circ, 24^\circ, 26^\circ, 28^\circ$ ) and compared with the traditional tee, respectively. As shown in Figure 9, when  $\theta = 18^\circ$ , the total resistance loss of the optimized tee increased by 136% compared with the traditional tee. With the increase of the angle of the guide plate, when  $\theta = 26^\circ$ , the total resistance loss of the optimized tee reached its minimum value of 0.53 and its maximum value of 72.4%. The resistance reduction effect of  $\theta = 26^\circ$  was the best.

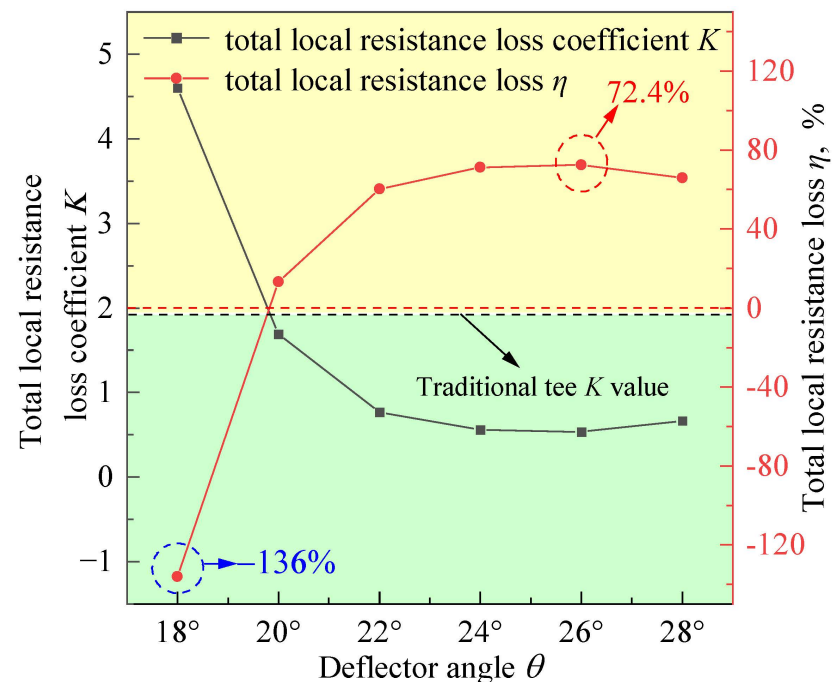


**Figure 9.** Total resistance loss coefficient diagram of the optimized tee.

### 3.2.2. Field Synergy Analysis

Based on the velocity field and pressure field results presented above, the volume-weighted average synergy angle of the traditional tee was calculated to be  $129.8^\circ$ . The volume-weighted average synergy angles  $\bar{\theta}$  of the six deflector angles in this study were  $127^\circ$ ,  $130^\circ$ ,  $130.1^\circ$ ,  $130.5^\circ$ ,  $130.8^\circ$ , and  $128.3^\circ$ , respectively, as shown in Figure 10. When  $\theta = 18^\circ$  and  $\theta = 28^\circ$ , the volume-weighted average synergy angle was smaller than that of the traditional tee. At this deflector angle, the deflector not only failed to guide the fluid to flow more adherently but also increased the eddy viscosity dissipation and did not have a resistance reduction effect. When  $\theta = 26^\circ$ , the maximum volume-weighted average synergy angle  $\bar{\theta}$  was  $130.7^\circ$ , which was  $1^\circ$  higher than that of the traditional tee.

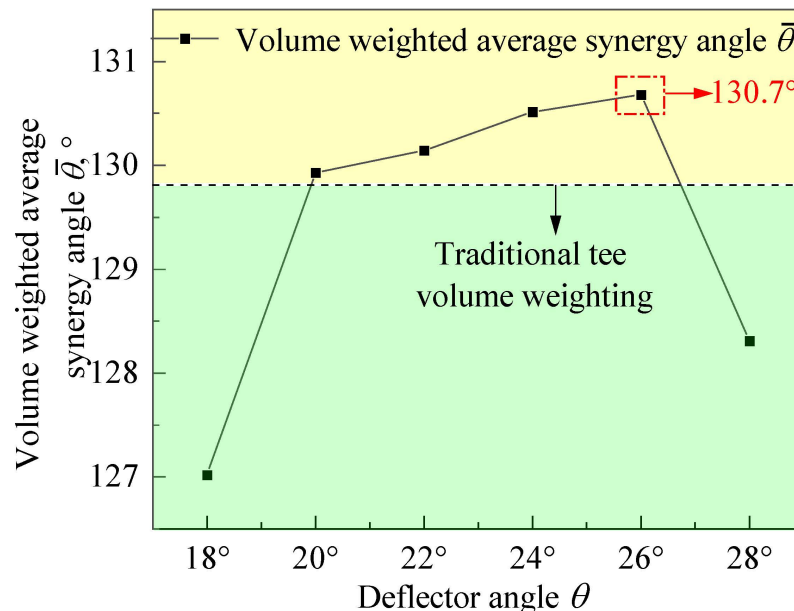


**Figure 10.** Volume-weighted average synergy angle diagram.

The volume-weighted average synergy for the best deflector angle  $\theta = 26^\circ$  was selected, and the synergistic effects of the deflector setting on the entire velocity field and pressure field were further explored. Twelve representative cross-sections were selected from the tee flow field, as shown in Figure 11. The cross-section average synergy angle  $\bar{\theta}'$  of the optimized tee was compared with that of the traditional tee, and the results are shown in Figure 12. The average synergy angles of the  $L_0$  and  $L_1$  circular sections in the main pipe section of the tee were greater than  $131^\circ$ , and the difference between the traditional and optimized tees was very small. This indicates that the deflector had little effect on the upstream flow. The section of straight pipe near the branch was impacted by the branch pipe. In both the optimized tee and the traditional tee, the synergy angle decreased suddenly, and the optimized tee was additionally affected by the deflector. The straight pipe flow experienced greater disturbance and the synergy angle was smaller. With the development of the flow pattern, the influence of the branch pipe and the deflector attenuated, the synergy angle increased, and  $L_6$  reached a maximum. In the branch pipe section where the local resistance was mainly reflected, the synergy angle of the optimized tee in the  $T_1$  section was smaller than that of the traditional tee. The synergy angle of the optimized tee in the  $T_2-T_4$  section was higher than that of the traditional tee, with an average increase of  $36^\circ$ . The maximum difference reached  $54^\circ$ , which appeared in the circular  $T_3$  section.

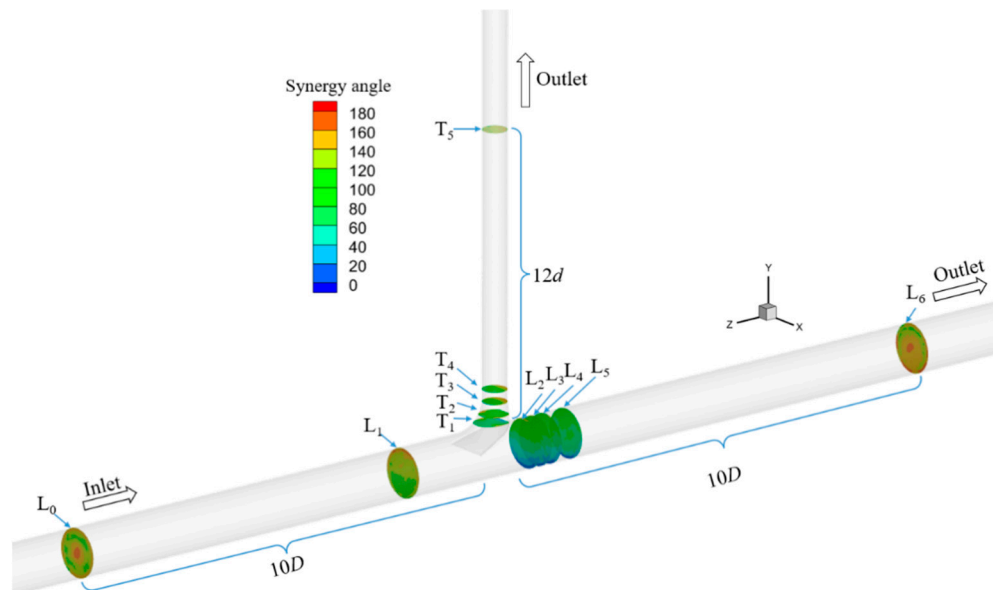


**Figure 11.** Optimization of the synergy angle distribution and position diagram of the tee's circular section.

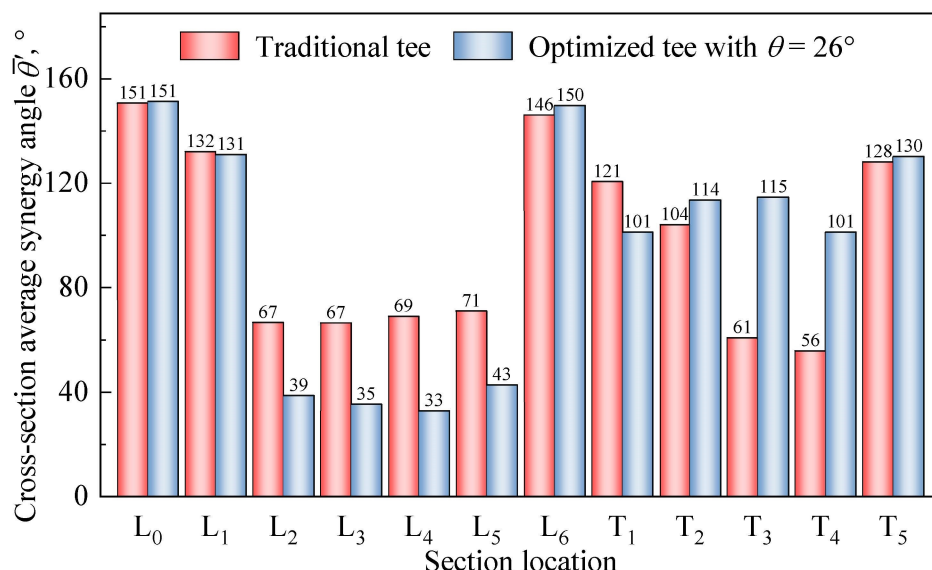


**Figure 12.** Comparison of the average synergy angle values of each circular section.

Throughout the field, the optimized tee was compared with the traditional tee synergy angle cloud map, as shown in Figure 13. The high-synergy-angle area at the center of the optimized tee main pipe increased, and the local synergy angle at the branch decreased slightly due to the addition of deflectors. However, it can be seen that the high-synergy-angle area downstream of the straight pipe increased significantly; the setting of the deflector caused a significant improvement in the synergy of the branch pipe flow. The synergy angle of the original maximum-velocity-gradient region in the branch pipe increased significantly, and the synergy of the overall velocity field and pressure gradient field of the branch pipe increased. Based on this analysis, the optimized tee's high-synergy-angle region was significantly greater than the traditional tee, and the pressure work efficiency improved.

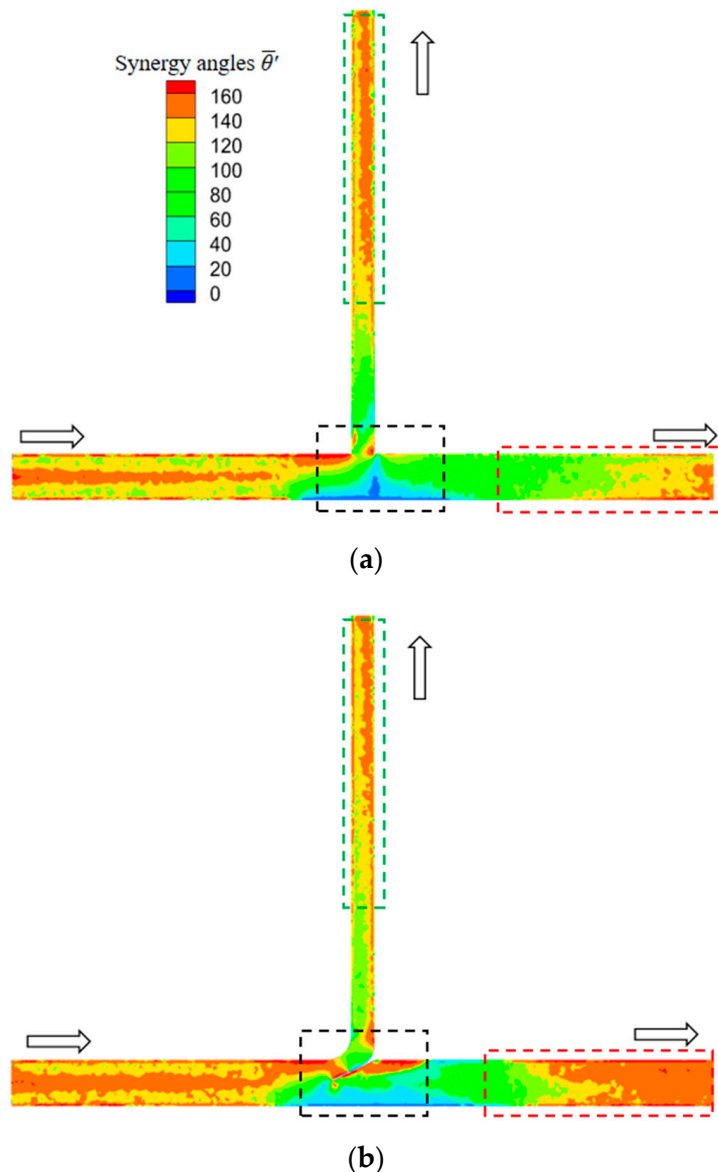


**Figure 13.** Synergy angle cloud diagram: (a) traditional tee; (b) optimized tee.

### 3.2.3. Viscous Dissipation Analysis

Through comparing the viscous dissipation distributions of the optimized tee and traditional tee, the resistance reduction effect was studied. As shown in Figure 14, when the fluid passes through the traditional tee, the viscous dissipation of the main pipe and the straight pipe is very small, and only a large viscous dissipation occurs at the wall of the pipe section. A large viscous dissipation was generated on the inner wall of the branch pipe,  $\Phi = 19.89$  W. Compared with the traditional tee, the optimized tee did not have any significantly high viscous dissipation regions, except for the pipe wall and the deflector. The deflector is equivalent to the wall surface for the fluid, so the energy dissipation near the deflector was relatively large, and the viscous dissipation inside the branch pipe was reduced,  $\Phi = 15.57$  W. After adding the deflector with  $\theta = 26^\circ$ , the viscous dissipation of the tee decreased by 21.7%.

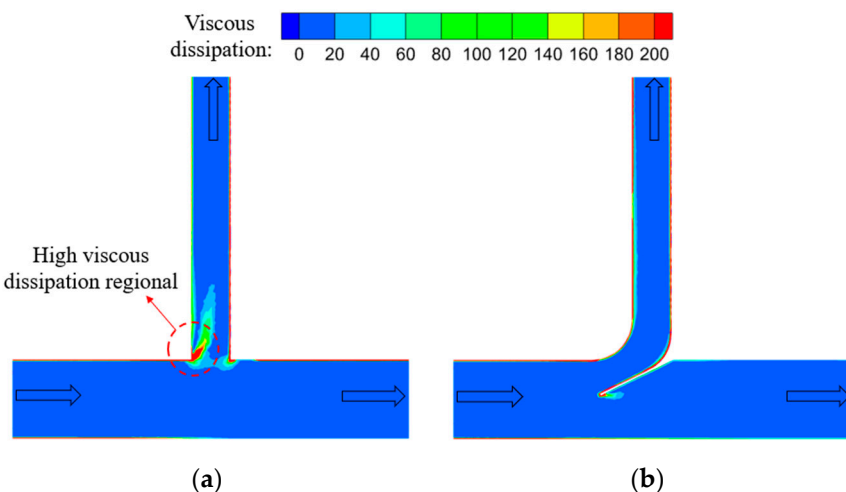


**Figure 14.** Viscous dissipation cloud diagram: (a) traditional tee; (b) optimized tee.

#### 4. Conclusions

In this work, the resistance characteristics and resistance reduction of the tee were analyzed through experiments and numerical simulations, and a novel tee with a U-shaped deflector was obtained. The resistance reduction effect of the U-shaped deflector angles was analyzed in detail based on the field synergy principle and the viscous dissipation principle. The resistance loss of novel and traditional tees was compared. The main conclusions are as follows:

- (1) The local resistance of the tee was mainly reflected in the flow separation and deformation of the fluid from the main pipe to the branch pipe. The relationship between the local resistance coefficient of the main branch pipe and the diameter ratio was exponential,  $\zeta_{01} = \alpha_1(d/D)^{\beta_1}$ , the local resistance coefficient of the main straight pipe was linear with the diameter ratio,  $\zeta_{02} = \alpha_2 \times (d/D) + \beta_2$ , and the selection of  $\alpha$  and  $\beta$  related to the split ratio.
- (2) The insertion of the tee branch disturbed the original axisymmetric flow. A large velocity gradient was generated in the boundary layer near the outer wall of the branch, and a reverse vortex flow even appeared near the inner wall. The velocity distribution offset and velocity gradient of the straight pipe section were relatively small. The non-uniform distribution of the velocity gradient in the tee provided a reference for the determination and optimization of the resistance reduction region.
- (3) After optimizing the wall of the tee and adding the guide plate, the resistance loss of the tee was effectively reduced, and the synergy of the fluid velocity and pressure gradient improved. The resistance reduction effect of the deflector with  $\theta = 26^\circ$  was the best, the total local resistance loss coefficient  $K$  was 0.53, and the total local resistance loss reduction rate  $\eta$  was the largest, at 72.4%. The maximum volume-weighted average synergy angle was  $130.7^\circ$ , which was  $1^\circ$  higher than that of the traditional tee. The viscous dissipation  $\Phi$  was 15.57 W, which was 21.7% lower than that of the traditional tee.
- (4) Further research is needed to investigate the impact of fluid types (such as petroleum and carbon dioxide gas) on the resistance of novel tee valves.

**Author Contributions:** Y.Y.: methodology, writing, original draft. C.S.: conceptualization, supervision, formal analysis. W.P.: validation, formal analysis. J.W.: visualization, formal analysis. Y.B.: visualization. All authors have read and agreed to the published version of the manuscript.

**Funding:** This work is funded by the Applied Basic Research Program of Shanxi (No. 202103021224091), the Applied Basic Research Program of Shanxi Province (No. 202203021212246) and the special fund for Science and Technology Innovation Teams of Shanxi Province (No. 202304051001011).

**Data Availability Statement:** The original contributions presented in the study are included in the article, further inquiries can be directed to the corresponding authors.

**Conflicts of Interest:** The authors declare no conflicts of interest.

## References

- Moran, P.; O’Connell, J.; Goggins, J. Sustainable energy efficiency retrofits as residential buildings move towards nearly zero energy building (NZEB) standards. *Energy Build.* **2020**, *211*, 109816. [[CrossRef](#)]
- Martínez-Molina, A.; Tort-Ausina, I.; Cho, S.; Vivancos, J.-L. Energy efficiency and thermal comfort in historic buildings: A review. *Renew. Sustain. Energy Rev.* **2016**, *61*, 70–85. [[CrossRef](#)]
- Skillington, K.; Crawford, R.H.; Warren-Myers, G.; Davidson, K. A review of existing policy for reducing embodied energy and greenhouse gas emissions of buildings. *Energy Pol.* **2022**, *168*, 112920. [[CrossRef](#)]
- Sinha, A.; Thakkar, H.; Rezaei, F.; Kawajiri, Y.; Realff, M.J. Reduced building energy consumption by combined indoor CO<sub>2</sub> and H<sub>2</sub>O composition control. *Appl. Energy* **2022**, *322*, 119526. [[CrossRef](#)]
- Feng, G.H.; Cui, H.; Chang, S.S.; Huang, K.L.; Wang, Q.R. Analysis of carbon emissions and influencing factors of near-zero energy buildings. *Clim. Chang. Res.* **2022**, *18*, 205–214.
- Li, Y.L.; Han, M.Y.; Liu, S.Y.; Chen, G.Q. Energy consumption and greenhouse gas emissions by buildings: A multi-scale perspective. *Build. Environ.* **2019**, *151*, 240–250. [[CrossRef](#)]
- Li, L.Y.; Sun, W.M.; Hu, W.; Sun, Y.K. Impact of natural and social environmental factors on building energy consumption: Based on bibliometrics. *J. Build. Eng.* **2021**, *37*, 102136. [[CrossRef](#)]
- P’erez-Lombard, L.; Ortiz, J.; Pout, C. A review on buildings energy consumption information. *Energy Build.* **2008**, *40*, 394–398. [[CrossRef](#)]
- Tang, Y.; Yu, H.; Zhang, K.; Niu, K.; Mao, H.; Luo, M. Thermal comfort performance and energy-efficiency evaluation of six personal heating/cooling devices. *Build. Environ.* **2022**, *217*, 109069. [[CrossRef](#)]
- Li, A.G.; Xi, C.; Lei, C.; Gao, R. Study on local drag reduction effects of wedge-shaped components in elbow and T-junction close-coupled pipes. *Build. Simul.* **2014**, *7*, 175–184. [[CrossRef](#)]
- Barth, W.L.; Branets, L.V.; Carey, G.F. Non-Newtonian flow in branched pipes and artery models. *Int. J. Numer.* **2010**, *57*, 531–553. [[CrossRef](#)]
- Beneš, L.; Louda, P.; Kozel, K.; Keslerova, R.; Stigler, J. Numerical simulations of flow through channels with T-junction. *Appl. Math. Comput.* **2013**, *219*, 7225–7235. [[CrossRef](#)]
- Gao, R.; Liu, K.K.; Li, A.G.; Fang, Z.Y.; Cong, B.H. Biomimetic duct tee for reducing the local resistance of a ventilation and air-conditioning system. *Build. Environ.* **2018**, *129*, 130–141. [[CrossRef](#)]
- Gao, R.; Zhang, H.C.; Li, A.G.; Liu, K.K.; Yu, S.R.; Deng, B.D. A novel low-resistance duct tee emulating a river course. *Build. Environ.* **2018**, *144*, 295–304. [[CrossRef](#)]
- Jing, R.Y.; Gao, R.; Zhang, Z.H.; Liu, M.C.; Liu, Y.F.; Zhu, W.L.; Zheng, Q.; Li, A.G. An anti-channeling flue tee with cycloidal guide vanes based on variational calculus. *Build. Environ.* **2021**, *205*, 108271.
- Gardel, A. Les pertes de charge dans les écoulements au travers de branchements en Té. *Bull. Tech. Suisse Rom.* **1957**, *9*, 123–130.
- Miller, D.S. *Internal Flow System*; BHRA; The Fluid Engineering Centre: Bedford, UK, 1990.
- Liu, T.X.; Li, S.T.; Jiang, C.; Zhang, X.; Tan, Z.J. Local Resistance Characteristics of T-Type Tee Based on Chamfering Treatment. *Sustainability* **2023**, *15*, 14611. [[CrossRef](#)]
- Han, F.H.; Ong, M.C.; Xing, Y.H.; Li, W.H. Three-dimensional numerical investigation of laminar flow in blind-tee pipes. *Ocean Eng.* **2020**, *217*, 107962. [[CrossRef](#)]
- Zhang, W.Q.; Li, A.G. Resistance reduction via guide vane in dividing manifold systems with parallel pipe arrays (DMS-PPA) based on analysis of energy dissipation. *Build. Environ.* **2018**, *139*, 189–198. [[CrossRef](#)]
- Gao, R.; Fang, Z.Y.; Li, A.G.; Liu, K.K.; Yang, Z.G.; Cong, B.H. A novel low-resistance tee of ventilation and air conditioning duct based on energy dissipation control. *Appl. Therm. Eng.* **2018**, *132*, 790–800. [[CrossRef](#)]
- Yin, Y.F.; Li, A.G.; Li, J.X.; Wu, D.M.; Wang, T.Q.; Ma, Y.Q.; Che, L.F. Analysis and optimization of energy loss reduction in a modified tee with deflectors via energy dissipation and vortex strength. *Energy Build.* **2023**, *290*, 113094. [[CrossRef](#)]
- Jing, R.Y.; Gao, R.; Liu, M.C.; Li, A.G.; Yu, S.R.; Xie, X.J.; Chen, C.J.; Zhou, M. A variable gradient descent shape optimization method for transition tee resistance reduction. *Build. Environ.* **2023**, *244*, 110735. [[CrossRef](#)]
- Guo, Z.Y.; Li, D.Y.; Wang, B.X. A novel concept for convective heat transfer enhancement. *Int. J. Heat Mass Trans.* **1998**, *41*, 2221–2225. [[CrossRef](#)]
- Guo, C.; Gao, M. Investigation on the flow-induced noise propagation mechanism of centrifugal pump based on flow and sound fields synergy concept. *Phys. Fluids* **2022**, *32*, 035115. [[CrossRef](#)]
- Liu, W.; Liu, P.; Dong, Z.M.; Yang, K.; Liu, Z.C. A study on the multi-field synergy principle of convective heat and mass transfer enhancement. *Int. J. Heat Mass Tran.* **2019**, *134*, 722–734. [[CrossRef](#)]
- Liu, X.F.; Zhao, Z.C.; Li, C.; Ding, J.H.; Pu, X.J. Investigation of local flow and heat transfer of supercritical LNG in airfoil channels with different vortex generators using field synergy principle. *Appl. Therm. Eng.* **2024**, *242*, 122424. [[CrossRef](#)]

28. Zhang, B.; Lv, J.S.; Zuo, J.X. Compressible fluid flow field synergy principle and its application to drag reduction in variable-cross-section pipeline. *Int. J. Heat Mass Transf.* **2014**, *77*, 1095–1101. [[CrossRef](#)]
29. Tong, Z.X.; Zou, T.T.; Jiang, T.; Yang, J.Q. Investigation of field synergy principle for convective heat transfer with temperature-dependent fluid properties. *Case Stud. Therm.* **2023**, *45*, 102926. [[CrossRef](#)]
30. Chen, Q.; Ren, J.X.; Guo, Z.Y. Fluid flow field synergy principle and its application to drag reduction. *Chin. Sci. Bull.* **2008**, *53*, 1768–1772. [[CrossRef](#)]
31. Yin, H.S.; Lei, Y.G.; Li, A.G.; Song, C.F.; Du, B.C. Field synergy principle for compressible laminar flow and the application for drag reduction in microchannel. *Phys. Fluids* **2022**, *34*, 116113. [[CrossRef](#)]
32. Yin, Y.F.; Li, A.G.; Wen, X.Q.; Zhang, J.W.; Zhang, X.; Guo, J.N.; Li, J.X.; Zhang, W.Q.; Che, J.G. Resistance reduction of an elbow with a guide vane based on the field synergy principle and viscous dissipation analysis. *J. Build. Eng.* **2022**, *54*, 104649. [[CrossRef](#)]
33. Gao, R.; Wang, M.; Wei, G.; Zhang, S.K.; Wen, S.H.; Wu, D.M.; Hang, Z.; Li, A.G. Study of the shape optimization of a variable diameter in a ventilation and air-conditioning duct based on the Boltzmann function. *J. Build. Eng.* **2021**, *43*, 102833. [[CrossRef](#)]
34. He, Y.L.; Lei, Y.G.; Tian, L.T.; Chu, P.; Liu, Z.B. An analysis of three-field synergy on heat transfer augmentation with low penalty of pressure drop. *J. Eng. Thermophys.* **2009**, *30*, 1904–1906.
35. Costa, N.P.; Maia, R.; Pinho, F.T.; Proenca, M.K. Edge Effects on the Flow Characteristics in a 90 deg Tee Junction. *J. Fluids Eng.* **2006**, *128*, 1204–1217. [[CrossRef](#)]

**Disclaimer/Publisher's Note:** The statements, opinions and data contained in all publications are solely those of the individual author(s) and contributor(s) and not of MDPI and/or the editor(s). MDPI and/or the editor(s) disclaim responsibility for any injury to people or property resulting from any ideas, methods, instructions or products referred to in the content.